Article

Investigation on Segregation Granulation by Fuel and Flux in Coating

Lin Wang [1,*], Xin Jiang [2,3,*], Qingyu Wang [2], Mingxing Ai [4], Xiaowei Yin [1], Jintao Liu [1] and Fengman Shen [2,3]

1   Department of Mechanical Engineering, Shenyang Institute of Engineering, Shenyang 110136, China
2   School of Metallurgy, Northeastern University, Shenyang 110819, China
3   Key Laboratory for Ecological Metallurgy of Multimetallic Mineral (Ministry of Education), Northeastern University, Shenyang 110819, China
4   Shandong Huizhe Environmental Protection Technology Co., Ltd., Rizhao 276800, China
*   Correspondence: wanglin@sie.edu.cn (L.W.); jiangx@smm.neu.edu.cn (X.J.)

Abstract: The metallurgical property of sinter is an important factor affecting the smooth operation of blast furnaces (BF), because it has a great impact on the permeability of BF and solid fuel rate. In order to promote the combustion of solid fuel and the mineralization of flux in sintering process, and eventually improve the strength of sintered ore, a series of investigation on segregation granulation by fuel and flux in coating were carried out, including the sinter pot experiments, the morphology analysis, and the discussion combine with phase diagram. The experimental results show that, (1) as the CaO increased from 0% to 40% and coke breeze increased from 0% to 100%, the sintering indices were improved, the tumble strength of sinter increased from 65.8% to 68.4%, the rate of qualified products increased from 77.4% to 81.0%, and the micro-strength of sinter increased from 68.7% to 75.9%. (2) There are three reasons for the high strength of sinter by segregation granulation of fuel and flux in coating, (a) the complete combustion of solid fuel and release the heat, (b) the effective absorb heat and mineralization of flux, and (c) the improvement of fluidity of bonding phase. The outcomes of the present work may provide a new method to improve the strength of sintered ore and give some reference for better understanding segregation granulation process and using it in actual operation.

Keywords: ironmaking; sinter; segregation granulation; coating; strength

1. Introduction

At present, the world's blast furnace iron production accounts for about 90% of the total production and the sinter in the blast furnace charge accounts for more than 75% [1]. The metallurgical property of sinter is an important factor affecting the smooth operation of blast furnaces [2,3]. In particular, it has the greatest impact on permeability of blast furnace and solid fuel rate. Therefore, optimizing the technical indices of sintering process and improving the metallurgical properties of sinter are crucial to the whole iron and steel smelting process. For this reason, scholars have carried out lots of investigations on improving the output and quality of sintered ore and reducing energy consumption.

Different iron ores have different physical and chemical properties and metallurgical properties in the sintering process. Applying the complementary principle of reasonable ore blending is an important and effective method to improve the quality of sintered ore [4–6], because it can improve the fluidity of liquid phase and the strength of the bonding phase of the sintered ore [7–10]. Jiang X et al. discussed the effects of liquidus temperature and liquid amount on the fluidity of bonding phase and the sintering strength of sinter [11]. Lv X F [12] et al. found that the sintered ore with good metallurgical properties can be obtained by reasonable ore blending according to the characteristics of iron ore itself. Zhang W H [13] et al. investigated the effects of the proportion of Canadian fine powder on the melting temperature of bonding phase, solid fuel consumption, and tumble strength of

sintered ore. Ou D M [14] et al. proposed that, by controlling the particle size of the solid fuel used in the sintering process, keeping the solid fuel particle size within a certain range can improve the combustion rate of solid fuel and make full use of solid fuel [15,16]. Loo C E [17] et al. analyzed the influence of size distribution of coke breeze on the permeability of sintering materials bed, temperature of combustion zone, sintering utilization coefficient, solid fuel consumption, and sintering speed, and metallurgical properties of sintered ore. It is pointed out that reasonable size of solid fuel is the key to ensuring yield, quality, and reducing solid fuel consumption. Wu S L [18] et al. showed that combustion with particle size larger than 3.15 mm is limited by the diffusion of oxygen and smaller than 1 mm is controlled by the kinetics of the $2C + O_2 \rightarrow 2CO$ reaction on the surface of carbon particles [19,20]. In the range of 1~3.15 mm it is controlled by both of them. It promotes the reaction on the surface of the carbon particles. It can not only make full use of solid fuel, but also the sintering speed and the strength of sintered ore is improved. Deep-bed sintering is a major development of sintering process in recent years due to the full use of the automatic heat storage of the layer. It has the advantage of reducing solid fuel consumption and improving the quality of sinter [21,22]. Nikolayev and Sato proposed the technical route of the double-layer (double combustion zone in the sintering bed) sintering method [23,24]. Zhou M S [25] et al. conducted an experimental study on the double-layer pre-sintering process and found that the oxygen-enriched operation can ensure the strength of the sinter, which proves that the process can increase the output of the sinter.

As mentioned in the literature, the research on sinter can be divided into three categories, (a) reasonable blending of different iron ores, (b) effective utilization of fuel and flux [26–28], and (c) some new sintering technologies and processes. In general, there are two key points in sintering process, one is the complete combustion of solid fuel and release of the heat, and the other one is the effective mineralization of flux. In order to strengthen these two points, a new segregation granulation technology by fuel and flux in coating was proposed by Nippon Steel Corporation (NSC) and they coined the term "quasi-particle" [29,30], and then, subsequently, some other Japanese plants development the technology. Oyama N [31] et al. investigated the influence of limestone and coke breeze distribution in the quasi-particle on permeability during sintering and sinter quality. Umadevi T [32] et al. investigated the influence of coating granulation process on iron ore sinter quality and productivity. Yang C C [33] et al. investigated the effectiveness granulation effectiveness of iron ore sinter feeds: effect of ore properties.

It is well known, under the different conditions, i.e., different iron ores, different fuel, and different flux, the optimal amounts of fuel and flux in coating are different. Therefore, in order to improve the strength of sinter and give some reference about quasi-particle to an ironmaking plant, the different amounts of fuel and flux in coating were investigated by sinter pot experiments under its actual raw material conditions. The outcomes of the present work may provide a new method to promote the combustion of solid fuel and the mineralization of flux in sintering process, and eventually improve the strength of sintered ore. Additionally, it can give some refers for better understanding segregation granulation process and using it in actual operation.

2. Materials and Methods

2.1. Raw Materials

The raw materials for sinter pot experiments mainly include iron ore fines, fuel and flux. In the sintering process, iron ores have different physical and chemical properties, and their sintering properties are also different, which can affect the sintering process and the quality of sinter. The sintering raw materials used in the present work were supplied by the Iron and Steel Company of China, including iron ore concentrate and fines, limestone, burnt lime, magnesite, and coke breeze etc. The chemical composition and proportion of the raw materials are listed in Table 1 and the particle size distribution are listed in Table 2. Among them, (1) Meishan is a kind of concentrate. (2) Newman, Hamersley, Chile and CVRD are imported hematite, and Yangdi is a limonite. (3) Magnesite is used to control the

MgO content in sinter and in BF slag. (4) Burnt lime and limestone were used to control the basicity of sinter, and limestone was used to control the content of CaO in the coating. The CaO in burnt lime accounted for about 60% in total CaO in the present proportion, and the CaO in limestone accounted for about 40% in total CaO. (5) The coke breeze was used as the solid fuel in the sintering process, and coke breeze was used to control the content of carbon in the coating.

Table 1. Chemical composition and proportion of raw materials (mass%).

No.	Raw Material	TFe	SiO_2	CaO	MgO	Al_2O_3	LOI	Proportion
1	Meishan	56.90	5.63	3.61	1.30	1.02	8.20	12.50
2	Newman	61.64	4.43	0.017	0.06	2.17	6.16	6.00
3	Yandi	57.9	4.56	0.29	0.11	1.85	10.28	13.00
4	Hamersley	62.00	3.54	0.09	0.034	2.28	3.33	15.20
5	Chile ore	66.26	2.06	0.46	0.59	0.60	1.02	3.00
6	CVRD	63.70	3.00	0.05	0.19	1.61	2.21	25.00
7	Return fines	57.00	4.86	8.90	1.90	1.22	0.29	10.00
8	Magnesite	0.00	3.80	2.38	36.37	0.50	47.22	4.60
9	Brunt lime	0.00	0.73	94.04	2.37	1.04	2.20	2.60
10	Limestone	0.00	3.50	50.98	0.69	0.80	41.10	3.50
11	Coke breeze	0.00	6. 09	0.74	0.45	3.90	85.17	4.60

Table 2. Particle size distribution of raw materials (mass%).

No.	Raw Material	Particle Size Distribution (Mass%)		
		−0.2 mm	0.2–1 mm	+1 mm
1	Meishan	99.82	0.1	0.08
2	Newman	19.75	24.27	55.98
3	Yandi	7.76	33.57	58.67
4	Hamersley	27.17	25.34	47.49
5	Chile ore	19.16	20.29	60.55
6	CVRD	15.25	24.23	60.52
7	Return fines	−5 mm (100%)		
8	Magnesite	−3 mm (100%)		
9	Brunt lime	−0.074 mm (100%)		
10	Limestone	−3 mm (100%)		
11	Coke breeze	−3 mm (100%)		

2.2. Experimental Design

In the present work, 5 sinter pot experiments were designed and listed in Table 3. It should be noted that brunt lime accounted for 2.6% of the total raw material (supply 60% of CaO to the mixture), and limestone accounted for 3.5% of the total raw material (supply 40% of CaO to the mixture). The proportion in Table 3 is the percentage of its own mass. In the table, No. 1 was the base period (no coating, 0% of CaO and coke breeze in coating), and the traditional granulation method was used. In the cases of No. 2 to No. 5, 25%, 50%, 75%, and 100% of limestone and coke breeze were added in coating, and corresponding 10%, 20%, 30%, and 40% of CaO were added in coating. In addition, SiO_2 content and binary basicity in the sintering mixture had crucial influences on the sintering characteristics. Based on the raw materials proportion in the sintering mixture

of the plant, the SiO_2 content of sinter was 4.95%, and the binary basicity was 1.90. In the segregation granulation, part of CaO was added in the coating and resulted in different basicity of quasi-particles. The binary basicity of quasi-particle was 1.90, 1.71, 1.52, 1.33, and 1.14, separately.

Table 3. Design for the sinter pot experiments on coating granulation.

No.	Burnt Lime		Limestone		CaO in Coating	Coke Breeze in Coating
	In Quasi-Particle	In Coating	In Quasi-Particle	In Coating		
1	100	0	100	0	0	0
2	100	0	75	25	10	25
3	100	0	50	50	20	50
4	100	0	25	75	30	75
5	100	0	0	100	40	100

2.3. Experimental Methods

2.3.1. Sinter Pot Experiments

The actual sintering conditions and process were simulated by the sintering pot experiments in the present work, and the flowchart of sinter pot experiments was shown in Figure 1. The sintering pot experiment mainly includes the following steps.
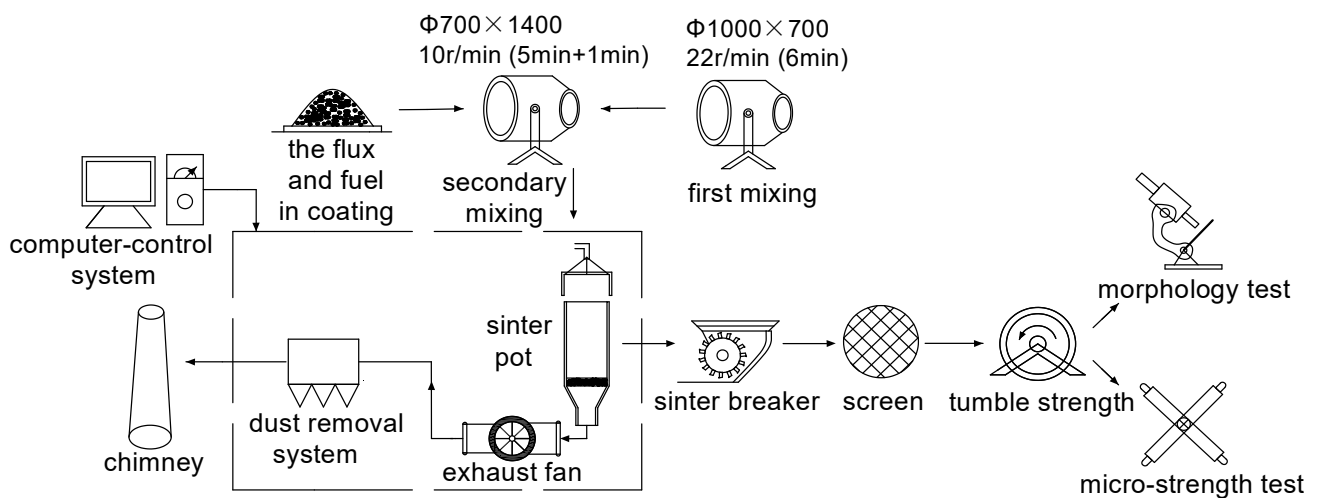
Figure 1. Flow chart of sinter pot experiments.

In the present work, two kinds of mixers were used. The specifications of the first mixer were Φ 1000 $\times$ 700 mm, rotating speed was 22 rmp, mixed for 6 min, the main purpose was to mix the raw materials. The specifications of the secondary mixer were Φ 700 $\times$ 1400 mm, rotating speed was 10 rmp, mixed for 5 min, the main purpose was granulation, and the limestone and coke breeze were added, as shown in Table 3, in the last 1 min. Water was sprayed by the nozzle in the mixer, and the mixing and spraying were carried out at the same time. In the actual sintering process, the size of the granulation should be neither too large nor too small. If the granulation is too large, the sintering speed is too fast, and results in lower strength of sinter. If the granulation is too small, the permeability of the material bed will become poor, and result in lower productivity. In the actual sintering process, 8% of water of the total mass is sprayed and all water is added in the first mixer. This ensures successful 3–8 mm of granulation and is accepted by almost any sintering plant.

(1)   Sintering process

The raw materials after first mixing and secondary mixing were loaded into the sintering pot. In the present work, the parameters of the sintering system are listed in Table 4.

Table 4. Parameters of sinter pot experiments.

Parameters	Values	Parameters	Values
Diameter of sinter pot	300 mm	Ignition temperature	1000 °C~1100 °C
Height of sintering bed	750 mm	Ignition time	2 min
Basicity of sinter	1.86	Pressure in ignition	7.0 kP
Moisture in the granulation	6.6%~6.8%	Pressure in sintering process	13.5 kP

(2)　Sintering indices test

(a)　Vertical sinter speed (*Vss*)

The vertical sintering speed *Vss* (mm/min) is shown in Equation (1).

$$Vss = \frac{H}{t} \times 100\% \tag{1}$$

In the Equation: *Vss*—vertical sintering speed, mm/min; *H*—the height of sintering bed, mm; *t*—sintering time, min.

(b)　Rate of qualified product (*Qp*)

After the sinter pot experiments, all of the sinter was put into a box which could be moved up and down automatically, and was moved up to a height of 2 m. Then, the sinter was free fallen on a steel plate from 2 m height. The test was repeated 3 times and the sinter was screened. The percentage (mass%) of +5 mm sinter to the total sinter was defined as the rate of qualified product, as shown in Equation

$$Qp = \frac{M_{+5} - M_H}{M - M_H} \times 100\% \tag{2}$$

In the Equation: *Qp*—rate of qualified product (mass%); M_{+5}—mass of +5 mm sinter; *M*—mass of total sinter; M_H—mass of hearth layer.

(c)　Tumble strength index (*TI*)

After the sinter pot experiments, 15 kg of 10–16 mm, 16–25 mm and 25–40 (take the corresponding ratio) sinter particles were put into a tumbler (Φ1000 × 500 mm). Then, the tumbler rotating speed was 25 rmp, rotating for 8 min (200 rotations). With a 6.5 mm square hole screen. After the screening, the ratio of the mass of +6.3 mm particles to the total particles was defined as the tumble strength index and denoted as *TI* (shown in Equation (3)).

$$TI = \frac{M_{+6.3}}{M} \times 100\% \tag{3}$$

In the Equation: *TI*—tumble strength index; $M_{+6.3}$—mass of +6.3 mm particles; *M*—total mass (15 kg).

2.3.2. Micro-Strength Tests

As shown in Figure 2, Usually, the bigger size and more samples are tested by tumble strength, and smaller size and little number of samples are tested by micro strength. It is an effective method to evaluate the strength of small particles. Next, 10 g of 1–3 mm sinter particles and 12 steel balls (8 mm in diameter) were put into a steel pipe (Φ25 × 300 mm). Then, the pipe rotating speed was 30 rmp for 10 min (300 rotations). After the rotation, the

ratio of the mass of +1 mm particles to the total particles was defined as the micro-strength and denoted as *Ms* (shown in Equation (4)).

$$Ms = \frac{M_{+1}}{M} \times 100\%$$ (4)

In the Equation: *Ms*—Micro-strength; M_{+1}—mass of +1 mm particles; *M*—mass of total sinter (10 g).

Figure 2. Micro-strength tests equipment.

2.3.3. Morphology Tests

The sinter was polished by setting them in an ethylenediamine-doped epoxy resin for the preparation of SEM-EDS analyses. SEM was performed using a JSM-6510LV scanning electron microscope (JEOL Ltd., Musashino, Akishima, Tokyo, Japan). The accelerating voltage was 20 kV. Energy-dispersive spectroscopy (EDS) was performed on this instrument.

2.3.4. Fluidity Tests

This part of the experiment was divided into three main steps.

(1)   Through calculation, the mixed ore powder with different proportions Fe_2O_3 and CaO was prepared. Weigh 1 g and put it into a mold with a diameter of 8 mm. The samples were prepared at a pressure of 12 MPa and kept for 3 min.
(2)   The preset temperature of the Equipment of melting point was set as 1280 °C. When the temperature rose to 1280 °C, the sample was put into the Equipment of melting point for heating.
(3)   The sample temperature also reached 1280 °C, the sample was kept at 1280 °C for 4 min, at which time, the sample would flow on the alumina sheet.

Figure 3. Schematic diagram of fluidity measured by the adhesive phase index. The multiple of the area after flow to the area before flow is defined as the fluidity index, as shown in Equation.

$$F = \frac{\frac{\pi \cdot X^2}{4}}{\frac{\pi \cdot \Phi^2}{4}} = \frac{X^2}{\Phi^2}$$ (5)

In the Equation: *F*—fluidity index; Φ—sample diameter before roasting, mm; *X*—diameter of the sample after roasting, mm.
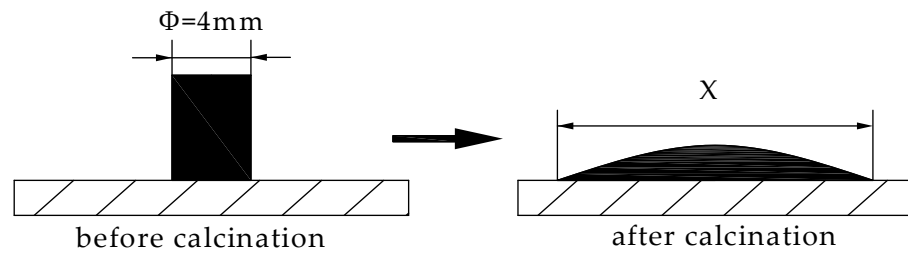
Figure 3. Schematic diagram of liquid phase fluidity index.

3. Experimental Results and Discussion

3.1. Sintering Indices

The sintering indices of sinter pot experiments, including tumble strength, rate of qualified product and sintering speed, are shown in Figure 4. It should be noted that the experimental No. in the figure corresponds to the experimental No. in Table 3 (the same below).
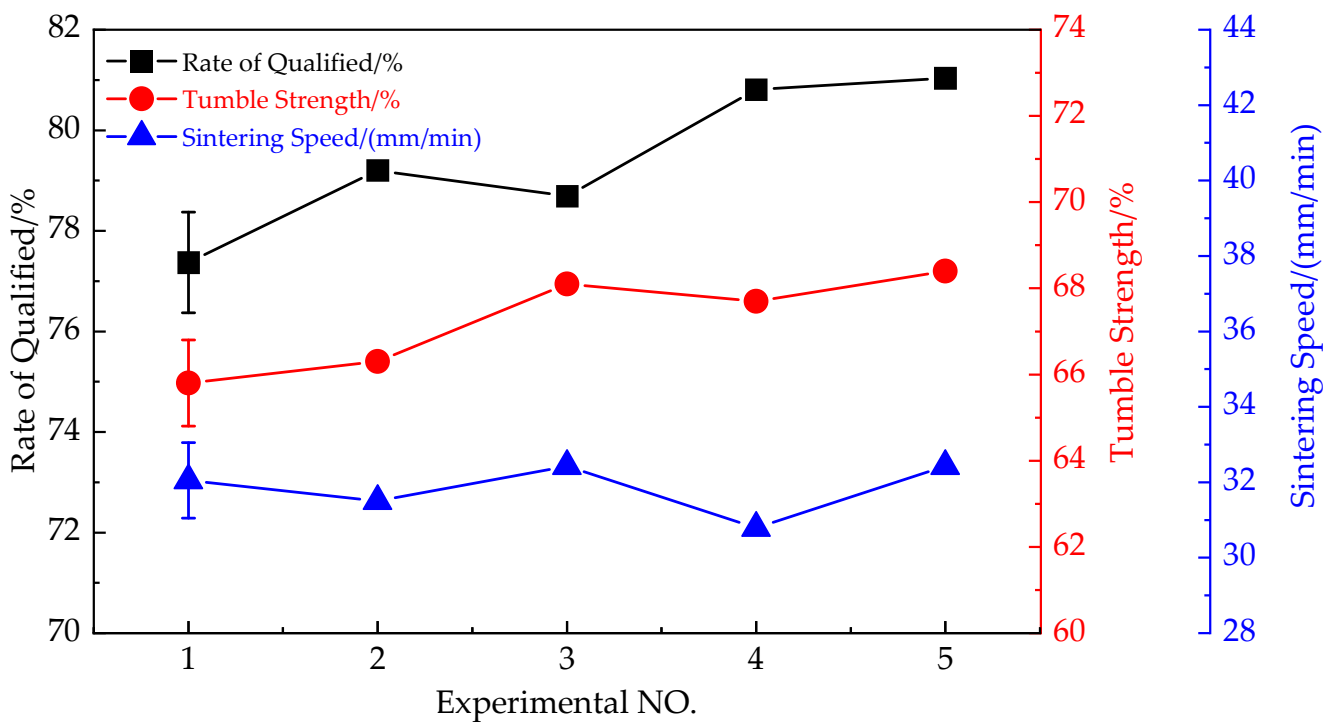

Figure 4. Sintering indices of sinter pot experiments.

From the Figure 4, one can conclude that, as the proportion of CaO increased from 0% to 40% and coke breeze increased from 0% to 100% (No. 1 to No. 5), the tumble strength increased from 65.80% to 68.40%, the rate of qualified product increased from 77.37% to 81.04%, and sintering speed had no obvious change.

3.2. Micro-Strength

The micro-strength of sinter is shown in Figure 5. From the Figure, one can conclude that, as the proportion of CaO increased from 0% to 40% and coke breeze increased from 0% to 100% (No. 1 to No. 5), the micro-strength increased from 68.69% to 75.90%.
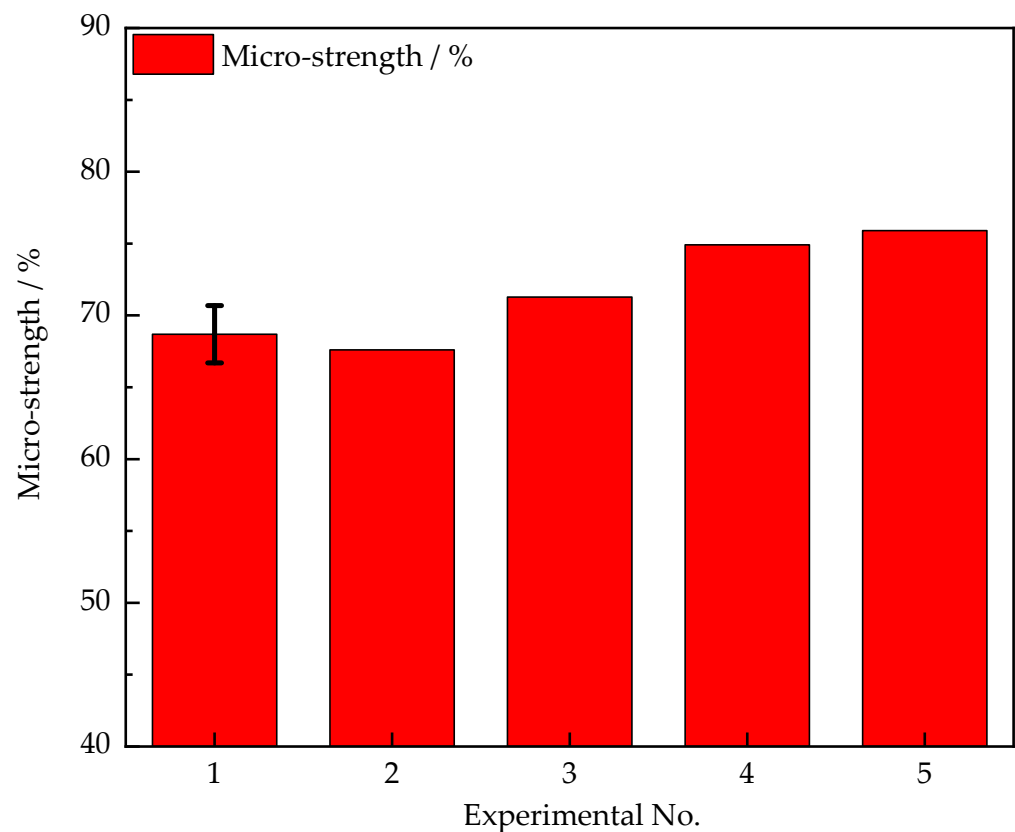
Figure 5. Micro-strength of sinter.

3.3. Morphology Analysis

The SEM of No. 1 sinter (0% of CaO and coke breeze in coating) is shown in Figure 6. The SEM-EDS analysis of typical sinter (Figure 6.) is shown in Figure 7. From the energy spectrum analyses, the contents of each element in point A, B, C could be obtained. The main component of point A is hematite. The main component of point B is Compound calcium ferrate (SFCA). The main component of point C is silicate.
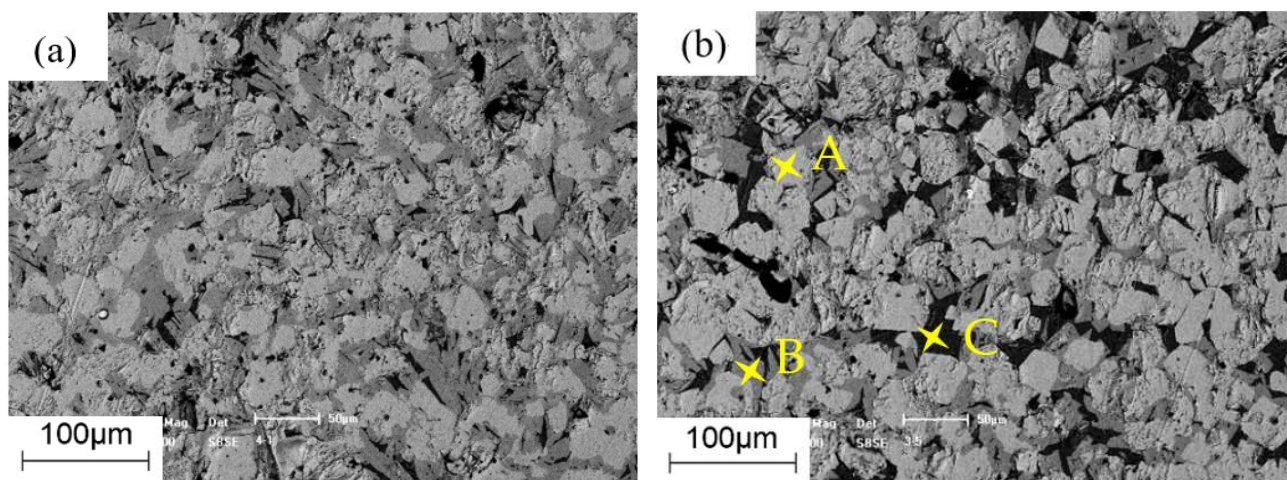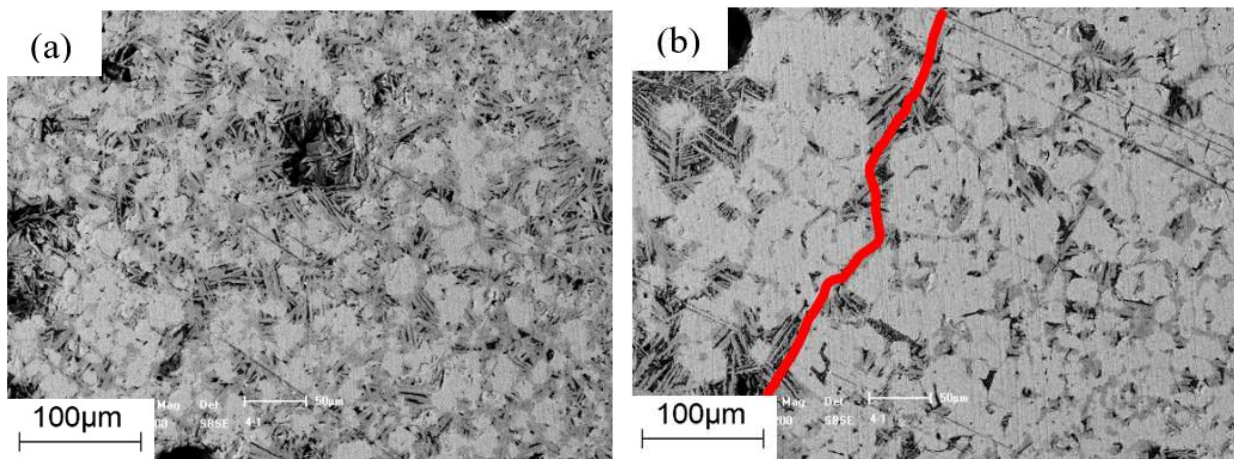

Figure 6. SEM of No. 1 sinter (0% of CaO and coke breeze in coating): (**a**) the mineral structure of the typical sinter, (**b**) a local part of the sinter.
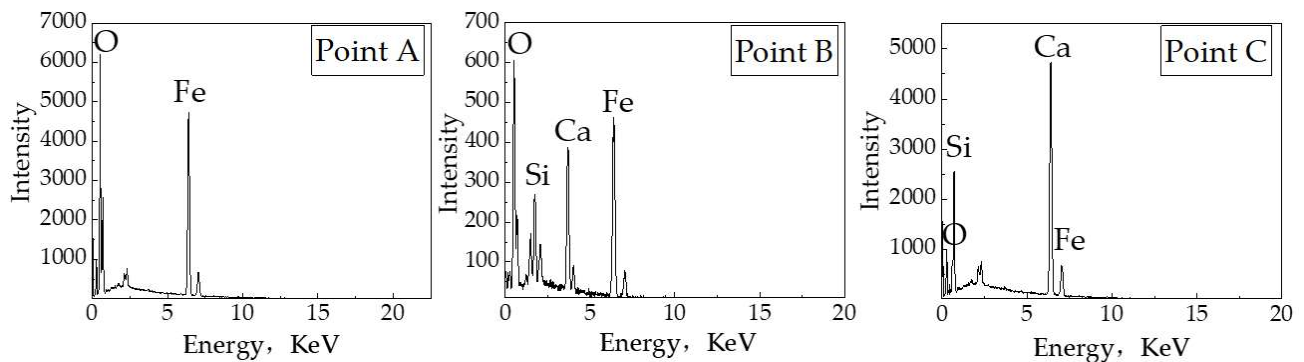
**Figure 7.** SEM-EDS analysis of typical sinter.

The mineral structure of the typical sinter is shown in Figure 6a. The un-melted hematite was wrapped in melted and crystalline SFCA bonding phase, forming a porous structure; a local part of the sinter is shown in Figure 6b. There was a lot of glass phase and little liquid phase. The liquid phase did not flow well. Most of them presented as columnar SFCA with poor contact with the ore. Existence of such a structure was the main reason for the poor strength of the sinter.

The SEM of No. 3 sinter (20% of CaO and 50% of coke breeze) is shown in Figure 8. The microstructure of the coating is shown in Figure 8a. There is more liquid phase in this part. Most of them presented as acicular SFCA with good contact with the ore. This can bond iron ores together and help to improve the strength of sinter. Microstructure of the interface between quasi-particle and coating is shown in the red line of Figure 8b. There was less liquid phase in the quasi-particle, and the sinter strength was supported by the crystallization of iron oxide itself (and a small amount of liquid phase). The sinter strength depended on how fully developed the bonding phase was in the coating.


Figure 8. SEM of No. 3 sinter (20% of CaO and 50% of coke breeze): (**a**) the microstructure of the coating, (**b**) the microstructure of the interface between quasi-particle and coating.

The SEM of No. 5 sinter (40% of CaO and 100% of coke breeze) is shown in Figure 9. The coating is shown in Figure 9a. There was more liquid phase, and more iron ore was melted into the liquid phase, improving the strength of sinter. The quasi-particle is shown in Figure 9b. There was less liquid phase, and the sinter strength was supported by the crystallization of iron oxide itself (and a small amount of liquid phase).
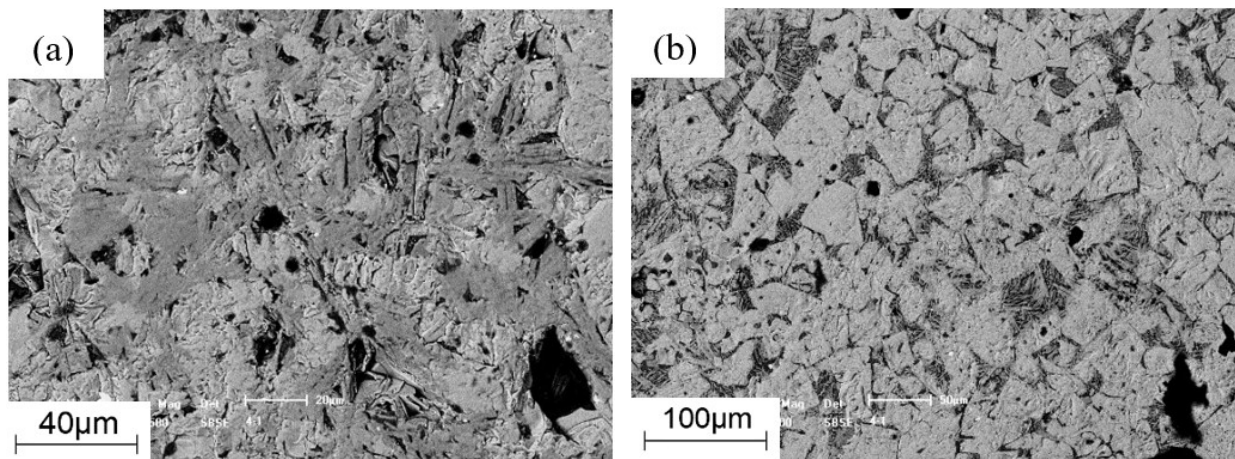
Figure 9. SEM of No. 5 sinter (40% of CaO and 100% of coke breeze): (**a**) the microstructure of the coating, (**b**) the microstructure of the quasi-particle.

Based on the composition and proportion of the raw materials, the CaO in burnt lime accounted for about 60% in total CaO in the granulation, and the CaO in limestone accounted for about 40%. The binding function of burnt lime was important for the granulation of the quasi-particle, and only the CaO in limestone could be added in the coating. Therefore, only 40% of CaO could be added in the coating. We wanted the test range of fuel to be as wide as possible, and then the 0% to 100% of coke breeze was designed. According to our experimental results, as the CaO increased from 0% to 40% and coke breeze increased from 0% to 100% (No. 1 to No. 5), the sintering indices were improved. However, it should be noted that in the part of No. 5 sinter (40% of CaO and 100% of coke breeze), there were some big pores and excessive liquid phase due to excessive solid fuel in the part of sinter, especially for the iron ores with high SiO_2 content, which are shown in Figure 10a,b. It is well known that the liquid phase also contains a SiO_2 component which will have a significant effect on the viscosity of liquid phase. More SiO_2 components may result in more big pores and excessive liquid phase. This kind of structure has a negative effect on the reducibility of sinter in blast furnace.
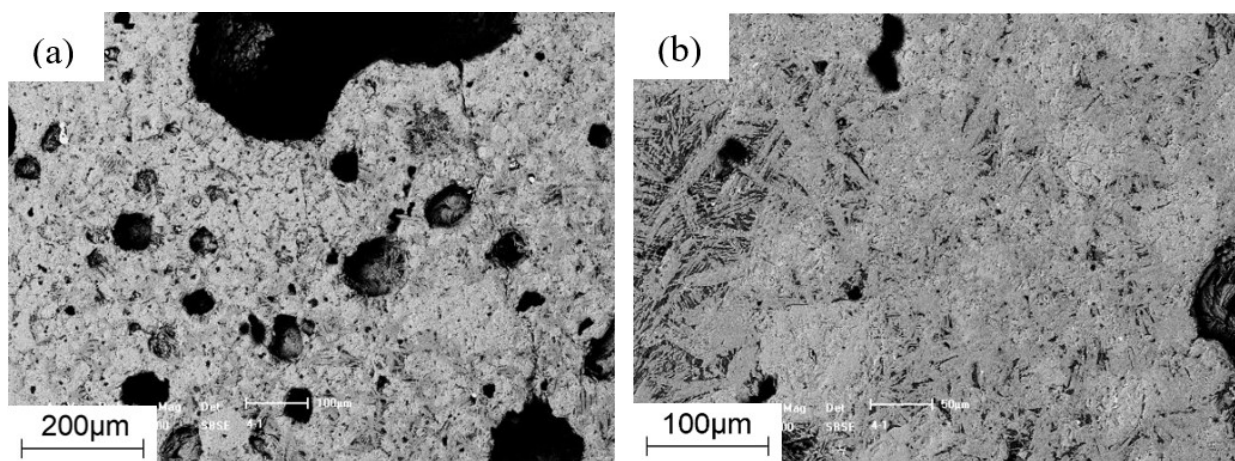

Figure 10. Big pores and excessive liquid phase in part of No. 5 sinter (40% of CaO and 100% of coke breeze): (**a**) the microstructure of some big pores, (**b**) the microstructure of excessive liquid phase.

3.4. Effect of Coating on the Fluidity of Bonding Phase

It is well known that the bonding phase in CaO-Fe_2O_3 binary system is the main bonding phase in sinter. The fluidity of bonding phase is controlled by the composition when the temperature is constant. In the present work, the fluidity of a series of bonding samples

were tested (Fe_2O_3 content were 72%, 74%, 76%, 78%, 80%, 82%, and 84% separately,). Figure 11 gives the testing results of the fluidity of bonding phase in CaO-Fe_2O_3 binary system. Figure 11 gives the fluidity of bonding phase in CaO-Fe_2O_3 binary system. All bonding phases in the present fluidity test (ranged between two red lines) were 100% of liquid phase in 1300 °C. One can conclude that the fluidity of the bonding phase decreased with the increase of Fe_2O_3 content. These results were consistent with the literatures, such as Han model [34], Iida model [35], etc. Therefore, in the process of coating granulation, some of fuel and flux were added in coating, which could have increased the CaO content and decreased the Fe_2O_3 content. Then, the fluidity of bonding phase increased, and it was positive for sintering process. Therefore, the improvement of fluidity of bonding phase was also one of the reasons for the fact that the sintering strength and the rate of qualified product increased with the amount of fuel and flux increased in coating.
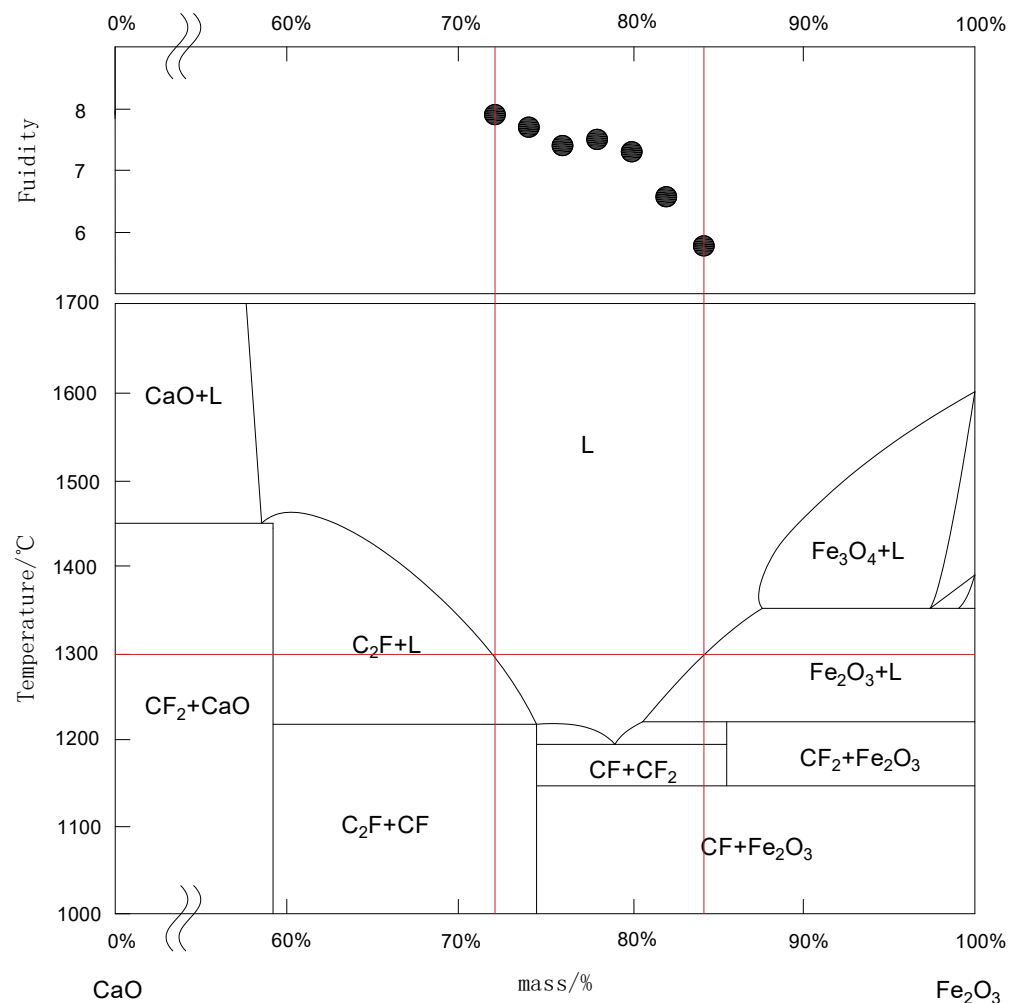
Figure 11. Fluidity of bonding phase in CaO-Fe_2O_3 binary system.

4. Conclusions

In this work, in order to promote the combustion of solid fuel and mineralization of flux in sintering process, a series of investigation on segregation granulation by fuel and flux in coating were carried out, including the amounts of fuel and flux by segregation granulation, the fluidity of bonding phase, and the microstructure of sintered ore. The main findings can be summarized as follows:

(1) As the CaO increased from 0% to 40% and coke breeze increased from 0% to 100% (No. 1 to No. 5), the sintering indices were improved, the tumble strength of sinter

increased 65.8% from to 68.4%, the rate of qualified products increased from 77.4% to 81.0%, and the micro-strength of sinter increased from 68.7% to 75.9%;

(2)　There were two reasons for the high strength of sinter by segregation granulation of fuel and flux in coating, (a) the effective absorption of heat and mineralization of flux, and (b) the improvement of fluidity of bonding phase, as the content of Fe_2O_3 in Fe_2O_3-CaO binary system decreased from 84% to 72%, the fluidity index increased from 5.8 to 7.9.

Author Contributions: Conceptualization, L.W. and X.J.; methodology, L.W. and X.J.; software, L.W. and X.J.; validation M.A. and X.Y.; formal analysis, L.W., X.J. and Q.W.; investigation, L.W.; resources, X.J.; data curation, L.W. and X.J.; writing—original draft preparation, Q.W.; writing—review and editing, F.S.; visualization, J.L.; supervision, F.S.; project administration, F.S.; funding acquisition, M.A. All authors have read and agreed to the published version of the manuscript.

References

1.　Gao, X.Y. Application Technology Development of Limonite in Sintering of Baogang. Master's Thesis, Inner Mongolia University of Technology, Inner Mongolia, China, 2021.
2.　Zhu, M.Y. *Modern Metallurgical Technology—Iron and Steel Metallurgy Volume*, 2nd ed.; Metallurgical Industry Press: Beijing, China, 2016; pp. 33–34.
3.　Liu, L.N.; Han, X.L. A Summary of Factors Affecting Sinter Quality. *J. HEBUT* **2006**, *28*, 18–21.
4.　Bi, X.G.; Wu, M.; Zhou, J.D.; Zhang, X.L. Development and Application of Optimized Blast Furnace Burdening. *Ironmaking* **2017**, *36*, 10–13.
5.　Zhang, Q.; Liu, R.; Wang, X.A.; Sun, Y.Q.; Lui, X.J. Optimization of the sintering proportioning of rich ore fines. *J. CQU* **2018**, *41*, 45–52.
6.　Yao, C.Q.; Zhang, J.L.; Zhang, Y.P.; Li, Z.J.; Li, X.Y. Sintering proportioning optimization based on high temperature performance of Tianjin Steel iron ore fines. *Sinter. Pelletizing* **2015**, *40*, 15–19.
7.　Zhang, J.L.; Hu, Z.W.; Zhou, H.B.; Lui, Z.J.; Zhao, Z.X.; Yang, T.Z. Ore blending ratio optimization for sintering based on iron ore properties and cost. *Ironmak. Steelmak.* **2014**, *41*, 279–285. [CrossRef]
8.　Zhang, D.S.; Gao, X.W.; Wang, Y.J.; Wang, M.S.; Ye, Y.J.; Tong, J.L. The Research of Sintering Ore Blending Based on Profit Maximization. In Proceedings of the 31st Chinese Control and Decision Conference, Nanchang, China, 3–5 June 2019.
9.　Lv, X.W.; Bai, C.G.; Deng, Q.Y.; Huang, X.B.; Qiu, G.B. Behavior of liquid phase formation during iron ores sintering. *ISIJ Int.* **2011**, *51*, 722–727. [CrossRef]
10.　Jiang, X.; Yu, J.X.; Wang, L.; Xiang, D.W.; Gao, Q.J.; Zheng, H.Y.; Shen, F.M. Distribution of reformed coke oven gas in shaft furnace. *J. Iron Steel Res. Int.* **2020**, *27*, 1382–1390. [CrossRef]
11.　Jiang, X.; Zhao, J.D.; Wang, L.; An, H.W.; Gao, Q.J.; Zheng, H.Y.; Shen, F.M. Effects of liquidus temperature and liquid amount on the fluidity of bonding phase and strength of sinter. *ISIJ Int.* **2021**, *61*, 86–92. [CrossRef]
12.　Lv, X.F.; Han, H.L.; Wu, S.L. Research on Ore-Proportioning Optimization Technology in Sintering. *Appl. Mech. Mater.* **2011**, *117*, 980–983. [CrossRef]
13.　Zhang, W.H.; Liu, H.L.; Sheng, H.L.; Wei, R.R.; Chen, N.G. Optimization of Sinter Ore Blending and Coping Practice of Blast Furnace. *Met. World* **2022**, *1*, 45–49.
14.　Ou, D.M.; Sun, Q.; Shen, H.B.; Yan, L.J.; Shi, H.Z. Effect of Coke Size on Iron Ore Sintering. *Iron. Steel.* **2008**, *43*, 8.
15.　Roberts, D.G.; Harris, D.J. A Kinetic Analysis of Coal Char Gasification Reactions at High Pressures. *Energ. Fuel.* **2006**, *20*, 2314–2320. [CrossRef]
16.　Roberts, D.G.; Harris, D.J. Char Gasification in Mixtures of CO_2 and H_2O Competition and Inhibition. *Fuel* **2007**, *86*, 2672–2678. [CrossRef]
17.　Loo, C.E. Role of Coke Size in Sintering of a Hematite Ore Blend. *Ironmak. Steelmak.* **1991**, *18*, 33.

18. Wu, S.L.; Chen, D.F.; Zhao, C.X.; Han, H.L.; Xue, F.; Zhang, L.H. Study on Improving Combustion. *Iron. Steel.* **2010**, *45*, 16–21.

19. Du, X.Y.; Goplakrishnan, C.; Annamalai, K. Ignition and Combustion of Coal particle Stream. *Fuel* **1995**, *74*, 487–494. [CrossRef]

20. Lockwood, F.C.; Mahmud, T.; Yehia, M.A. Simulation of Pulverized Coal Test Furnace Performance. *Fuel* **1998**, *77*, 1329–1337. [CrossRef]

21. Zhai, J.N. Economic Analysis of Baosteel's deep bed sintering Technology Innovation. Master's Thesis, Central South University, Hunan, China, 2005.

22. Wang, D.J.; Wu, S.L.; Li, C.J.; Zhu, J. Efficient and Clean Production Practice of Large-Scale Sintering Machine. *ISIJ Int.* **2013**, *53*, 1665–1672. [CrossRef]

23. Liu, J.; Zhou, M.S.; Wu, F.D.; Zhang, H.; Xu, L.B.; Zhai, L.W.; Gao, W.; Zhong, Q. Study of the Double-Layer Sintering Process with Stand-Support. *Metal* **2022**, *12*, 629. [CrossRef]

24. Sato, S.; Kawaguchi, T.; Kato, M. Lower limit of the energy consumption and the double ignition process for iron ore sintering. *ISIJ* **1988**, *28*, 705–713. [CrossRef]

25. Zhou, M.S.; Wang, Y.D.; Han, S.F.; Zhao, D.M.; Zhu, J.W. Research and industrial test on ultra-deep bed double-layer pre-sintering process. *Sinter. Pelletizing* **2019**, *44*, 23–27.

26. Jiang, X.; An, H.W.; Han, H.S.; Ding, X.; Li, L.S.; Shen, F.M. Reaction characteristics between sinter and serpentine. *Metall. Mater. Trans. B* **2020**, *51*, 937–944. [CrossRef]

27. Jiang, X.; Zhang, H.Y.; Zheng, H.Y.; Gao, Q.J.; Shen, F.M. Three-segment control theory of MgO/Al_2O_3 ratio based on viscosity experiments and phase diagram analyses at 1500 °C. *J. Iron Steel Res. Int.* **2020**, *27*, 624–630. [CrossRef]

28. Balat, M. Influence of coal as an energy source on environmental pollution. *Energy Sources* **2007**, *29*, 581–589. [CrossRef]

29. Hida, Y.; Sasaki, M.; Enokido, T.; Umezu, Y.; Iida, T.; Uno, S. Effect of Existing State of Coke Breeze in Quasi-Particles of Raw Mix on Coke Combustion in the Sintering Process. *Tetsu-to-Hagang* **1982**, *68*, 400–409. [CrossRef] [PubMed]

30. Hida, Y.; Miyazaki, T.; Sasaki, M.; Soma, K.; Naito, H.; Kagawa, M. Study on sintering of iron ore with advanced analyzers (production of high-reducibility sinter with low fuel consumption). *Overseas* **1987**, *35*, 59–67.

31. Oyama, N.; Igawa, K.; Takena, J.; Ariyama, T.; Jinno, T. Influence of Limestone and Coke Breeze Distribution in the Quasi-particle on Permeability during Sintering and Sinter Quality. *Tetsu-to-Hagang* **2004**, *90*, 546–553. [CrossRef]

32. Umadevi, T.; Deodhar, A.V.; Mahapatra, P.C.; Prabhu, M.; Ranjan, M. Influence of Coating Granulation Process on Iron Ore Sinter Quality and Productivity. *Steel Res. Int.* **2010**, *81*, 717–723. [CrossRef]

33. Yang, C.C.; Zhu, D.; Pan, J.; Lu, L. Granulation Effectiveness of Iron Ore Sinter Feeds: Effect of Ore Properties. *ISIJ Int.* **2018**, *58*, 1427–1436. [CrossRef]

34. Han, C.; Chen, M.; Zhang, W.; Zhao, Z.; Evans, T.; Nguyen, A.T.; Zhao, B.J. Viscosity model for iron blast furnace slags in SiO_2-Al_2O_3-CaO-MgO System. *Steel Res. Int.* **2015**, *86*, 678–685. [CrossRef]

35. Iida, T.; Sakai, H.; Kita, Y. An Equation for accurate prediction of the viscosities of blast furnace type slags form chemical composition. *ISIJ Int.* **2000**, *40*, 110–114. [CrossRef] [PubMed]